In Terahertz and Gigahertz Electronics and Photonics IV, edited by R. Jennifer Hwu and Kurt J. Linden, Proc SPIE 5727, 44-53 (2005). Photonics West 2005, San Jose CA

# Amplification of terahertz radiation in delta-doped germanium thin films

A.V. Muravjov [a, *)], M. V. Dolguikh [a)] R. E. Peale [a)], O. A. Kuznetsov [b)], E. A. Uskova [b)]

[a)] Department of Physics, University of Central Florida, Orlando FL, 32816.
[b)] Physical-Technical Research Institute, Nizhny Novgorod State University, Russia, 603950.
[*)] On leave from the Institute for Physics of Microstructures, RAS, Nizhny Novgorod, Russia.

## ABSTRACT

A new geometry for the intersubband THz laser on delta-doped multi-layer Ge thin films with in-plane transport of carriers in crossed electric and magnetic fields is proposed. A remarkable increase of the gain compared to existing bulk p-Ge lasers is based on spatial separation of light and heavy hole streams, which helps to eliminate scattering of light holes on ionized impurities and the majority of heavy holes. Inversion population and the gain have been studied using Monte-Carlo simulation. The terahertz transparency of a CVD-grown delta-doped Ge test structure has been experimentally studied by intracavity laser absorption spectroscopy using a bulk p-Ge laser. A practical goal of this study is development of a widely tunable (2-4 THz) laser based on intersubband hole transitions in thin germanium films with the gain sufficient to operate at liquid nitrogen temperatures.

**Keywords:** terahertz laser, germanium, delta-doped, intersubband, Monte-Carlo

## 1. INTRODUCTION

The mechanism of generation of THz stimulated emission on direct optical transitions between subbands of the valence band in bulk semiconductors in crossed E and B fields, well known for bulk p-Ge lasers [1], has several limitations which lead to low efficiency and liquid helium temperatures requirements for the laser operation. These limitations are mainly caused by insufficient gain in the face of lattice absorption, which grows rapidly with temperature, and the negative impact of impurity scattering at high doping concentrations.

In this paper we propose a new in-plane configuration of the intersubband THz laser on delta-doped multi-layer Ge thin films, based on spatial separation of light and heavy hole streams, that allows remarkable increase of the gain in comparison with bulk p-Ge lasers. This configuration uses planar hole transport and differs from our previously published delta-doped p-Ge laser design with vertical transport [2,3]. Theoretical and experimental analysis of the hot hole dynamics and inversion population in crossed E and B fields in selectively doped structures is presented. Our practical goal is development of a terahertz laser based on thin germanium films with small signal gain coefficient sufficient to operate at liquid nitrogen temperatures. An additional motivating factor for pursuing our approach, when THz quantum cascade lasers have already achieved this temperature milestone [4,5], is the unique very wide gain spectrum (2-4 THz) for the transitions between subbands of the valence band. This feature is potentially important for building a terahertz laser with wide tunability, which none of the other known terahertz semiconductor lasers possesses.

The mechanism of building up the population inversion in p-type Germanium in crossed electric and magnetic fields is presented in Fig.1. Due to different effective masses, the ratio between the magnitudes of applied electric and magnetic fields can be chosen (typically E=1.5 kV/cm and B=1T), so that light holes become confined on cyclotron trajectories below the optical phonon energy threshold, while heavy hole trajectories are only slightly affected by the magnetic field, allowing them to intensively scatter with emission of optical phonons. The lifetime of magnetized light holes, which defines the population inversion, depends on three major scattering processes. *Acoustic phonon* scattering increases with lattice temperature and tends to thermalize the non-equilibrium hole distribution. This is one reason why p-Ge lasers require low temperatures. More importantly, acoustic phonons contribute to lattice absorption of THz radiation. If the laser is to operate at liquid nitrogen temperature (77 K), the THz gain needs to be sufficient to overcome this absorption, which so far has not been possible in traditional bulk p-Ge lasers. Scattering of light holes on *ionized*

*impurities* limits the maximum acceptable concentration of acceptors, and thus the concentration of active carriers to the level of $1\sim2\times10^{14}$ cm$^{-3}$, so that the gain has not exceeded 0.1- 0.2 cm$^{-1}$ in homogeneously doped p-Ge lasers. *Carrier-carrier* collisions cause intersubband and intrasubband scattering similar to ionized impurity scattering, but adequate analysis for high concentration in the conditions of degenerate bands has not been done until now.

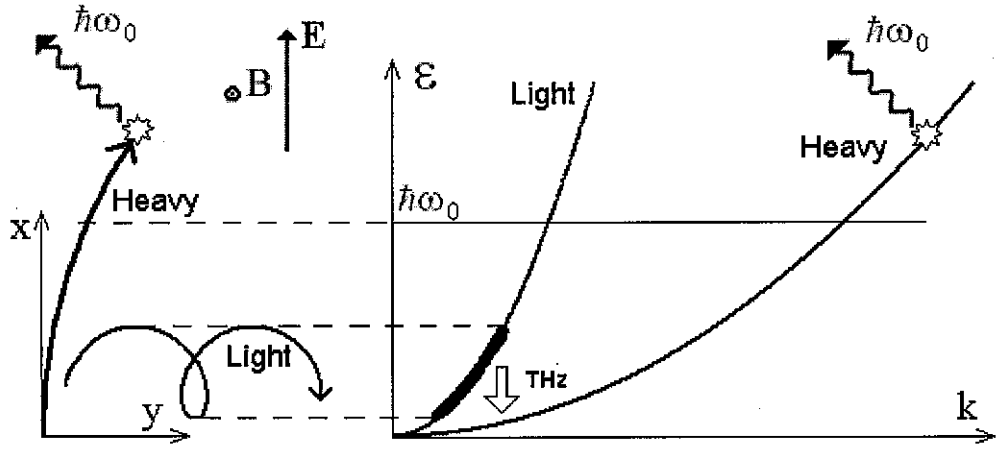


Fig.1. The mechanism of stimulated emission on direct optical transitions between light and heavy hole subbands. The left graph shows light and heavy hole orbits in the plane perpendicular to the applied magnetic field. The right figure shows the allowed energies of light and heavy holes as a function of the magnitude of the momentum wavevector. Heavy holes scatter rapidly with optical phonon emission. Light holes are magnetized, have much smaller collision rates, and therefore have a long life time. Overpopulation of the light hole subband results in THz gain on direct optical light-to-heavy hole transitions.

## 2. BASIC CONCEPTS

Recently we proposed a concept of the terahertz intersubband hot hole laser based on multi-layer selectively doped Ge structures with vertical carrier transport [2,3]. In contrast to bulk p-Ge laser with randomly uniform acceptor distribution we used delta-doped layers with a period larger than light-hole cyclotron radii, allowing light holes to accumulate in the regions between the doped layers free from ionized impurity scattering. This factor allows an increase in the total average concentration of carriers to $5 \times 10^{14}$ cm$^{-3}$, in contrast to the optimal level $1 \times 10^{14}$ cm$^{-3}$ for the bulk p-Ge lasers. A THz gain of 0.5 cm$^{-1}$ is anticipated. The main mechanism which limits the light hole populations in these devices is hole-hole scattering, which must be treated accurately. In Appendix we made detailed analysis of hole-hole scattering in approximation of two degenerate hole bands with isotropic and parabolic dispersion law and found the non-radiative intersubband scattering rates for light holes related to hole-hole scattering.

Fig. 2 compares the total rate of light-to-heavy hole intersubband transitions for a light hole scattering on heavy holes or on ionized impurities. The rates have been integrated over calculated light and heavy hole distribution functions in p-Ge at 10 K for applied electric and magnetic fields of 1.5 kV/cm and 1.1 T, respectively. Results for two different kinetic energies of the incident light hole are presented. Transition rates appear to be lower for carrier-carrier scattering than for ionized impurity scattering by the factor ~ 1.5. This latter point supports the claimed advantage of the proposed device structure, which separates impurity centers from light hole accumulation regions yet cannot so easily remove the heavy holes. Though heavy holes remain in the undoped regions their negative effect on the inversion population is less severe than that of ionized impurity centers.

An alternative configuration of the active delta-doped germanium structure and applied fields, which achieves spatial separation of light holes from *both* impurity and heavy holes is presented in Fig.3. The magnetic field is oriented along the layers. The orientation of electric field is chosen to keep heavy hole current $j_h$ within the doped layers. Heavy holes

trajectories are shown dark and located in the close vicinity of the doped layers. Light holes (grey) move across the doped layers due to the drift in the direction perpendicular to both applied electric and magnetic fields. By this mean the concentration of light holes in the active regions between the doped layers can be achieved more than 50% of the total hole concentration. The picture on Fig. 3 presents the pattern of hole trajectories from the actual Monte-Carlo simulation at E=3 kV/cm, B=2T, T=10K, average hole concentration 1.5 x $10^{15}$ $cm^{-3}$, and structure period d=2000 nm.

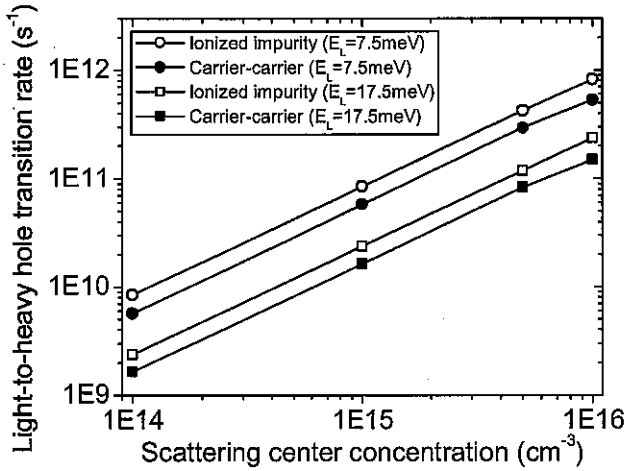


Fig. 2 Rates of downward intersubband transitions for scattering of light holes on heavy holes or ionized impurities versus concentration of scattering centers calculated for typical p-Ge laser hole distribution functions. Results are presented for for two different light hole energies.

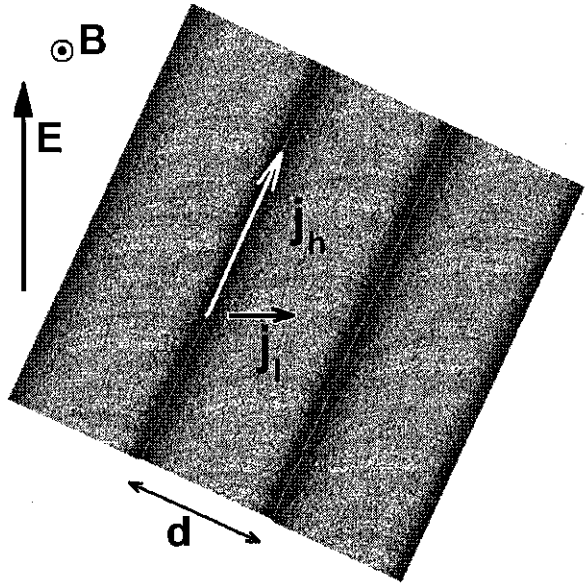


Fig. 3 Computer simulated hole trajectories in the delta-doped structure in crossed electric and magnetic fields.
E = 3 kV/cm, B= 2T, d= 2000 nm, average hole concentration 1.5 x $10^{15}$ $cm^{-3}$.

Fig.4 presents the spatial dependence of light and heavy hole concentration profile across the period of the structure. In the central part of the structure the average absolute concentration of light holes reaches the value 1-2 x $10^{14}$ $cm^{-3}$, which is comparable or even higher than the heavy hole concentration. Taking into account that filling factor of the states in different subbands is in inverse proportion to their densities of states, the light hole subband is a factor of ($m_{h/}$

$m_l)^{3/2}$ ~ 23 times more populated higher than the heavy hole subband. That corresponds to remarkable local inversion population on direct optical transitions and the local THz gain may reach a value of several $cm^{-1}$. The spatially averaged net gain in the structure, however, is rather low because of the strong free carrier absorption in the aria around delta-doped layers with high concentration of heavy holes. Fig.5 shows the result of the calculation of the total gain with and without free carrier absorption.

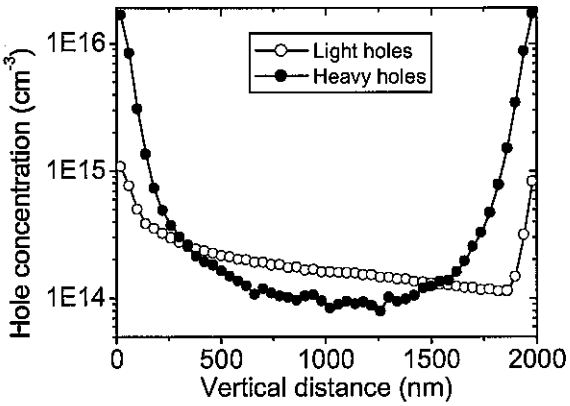


Fig.4 Distribution of light and heavy hole concentrations across the period of the structure.

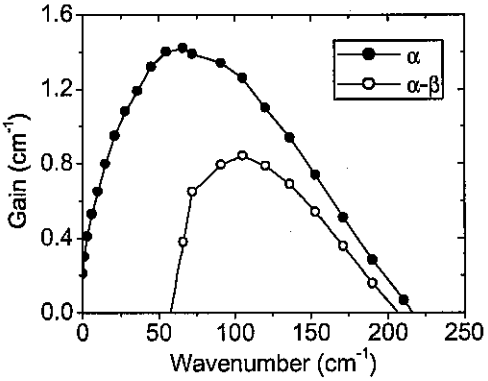


Fig.5 Calculated spatially averaged terahertz gain α in the structure with parameters as for Fig. 3. The net curve α-β includes the free carrier absorption coefficient.

Calculations of the gain for different applied fields and structure periods confirm the expectation that the optimal period of the structure for the maximum average gain should approximately equal to the mean free pass of the light holes. For parameters as in Figs. 3-5 the light hole mean free pass is about 2 μm, which can be seen in fig.4 from the exponential decrease of the light hole concentration with the vertical distance from the doped layers. Attempts to increase the distance *d* between the doped layers to the scale comparable to one half the wavelength of the generated emission, in order to apply waveguide electrodynamic solutions, leads to a decrease of the light hole population in the gap and lower gain.

## 3. EXPERIMENTAL METHODS

First test structures were grown by CVD with thickness from 14 to 33 μm and average doping concentrations of the order of $10^{16}$~$10^{17}$ $cm^{-3}$. This concentration is still higher than the optimal $10^{15}$ $cm^{-3}$ for the laser emission, but these structures allowed us to adjust all growth parameters. The thickest one consists of 90 delta-doped periods. Fig. 6 shows Secondary Ion Mass Spectrometer (SIMS) data for a structure with 35 periods and a 14 μm thickness. Growth duration

was about 1 hour. The linear SIMS spectrum on Fig. 6 (right) shows more clearly the doping profile, which show that diffusion of Boron acceptors from doped layers during CVD growth is insignificant.

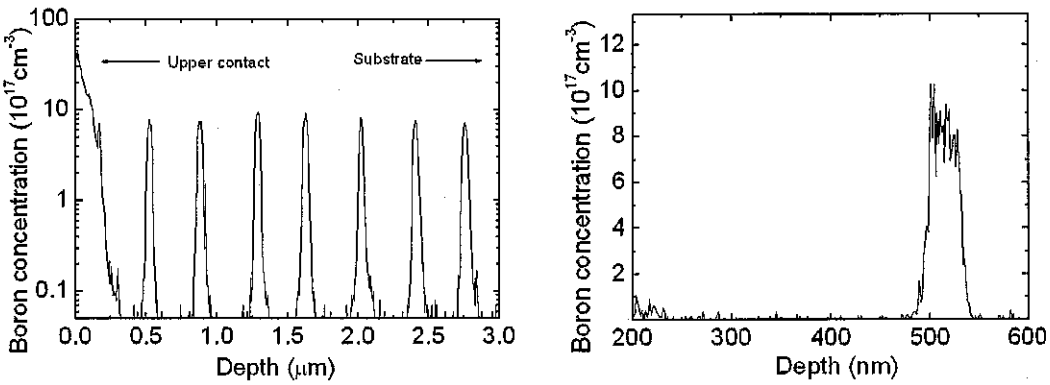


Fig 6 Left: Semi-logarithmic SIMS spectrum of boron for first 7 periods of a CVD-grown 35 period p+Ge/Ge structure. The intentional high boron concentration on the surface is the contact layer. Right: Linear SIMS spectrum of the first period of the structure to determine the impurity diffusion profile.

In order to study THz transparency of the grown structure we used a method of intracavity laser transmission using a bulk p-Ge laser operating in the frequency range 2-4 THz. Fig. 7 shows a schematic of the intracavity laser absorption measurement. The laser crystal is Ga doped to concentration 7 x $10^{13}$ cm$^{-3}$ with long axis along <110> and electric field applied along <1-10>. Electric field $E_1$ in the range 1-2 kV/cm is applied in 1 microsecond pulses with a thyrotron pulser to GaIn ohmic contacts. Electric field $E_2$ is applied with an IGBT pulser in microsecond pulses to GaIn contacts on two opposite edge faces of the structure. The back surface of its undoped 200 μm-thick substrate, oriented in <111> crystallographic direction, was polished parallel to the surface with the epilayers. The magnetic field B in the range 0.5 to 1.5 T is applied using a superconducting solenoid, which is immersed in liquid helium. The Ge:Ga detector is biased (and saturates) at 1.3 V.

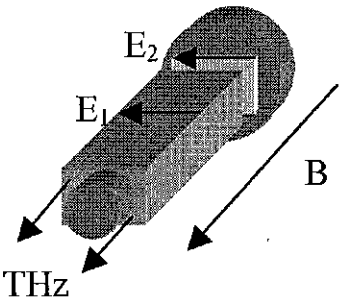


Fig. 7 Schematic of intracavity laser absorption spectroscopy. Electric field $E_1$ is applied to the p-Ge laser crystal. Electric field $E_2$ is independently applied to the multilayer delta-doped structure. The magnetic field B is applied parallel to the long axis in Faraday configuration. Copper mirrors are attached to the parallel end faces of the compound laser assembly. The output coupling mirror is smaller than the laser end face to allow THz emission output, which is detected with a Ge:Ga photoconductor.

Because the investigated structure was located directly inside the p-Ge laser cavity in the close vicinity to the active p-Ge laser sample, the magnetic field applied to the laser crystal and the structure is the same. The configuration of applied electric and magnetic field in this experiment corresponds to Faraday configuration, which is different from the detailed theoretical results presented above for Voigt configuration. However, this experiment provided information about THz transparency of the substrate, quality of optical surfaces, level of free carrier absorption and the feasibility of the method of intracavity p-Ge laser spectroscopy for future investigation of the delta-doped structures.

Fig. 8 shows dependence of the intensity of p-Ge laser radiation (scale on the right) as a function of the electric field applied to the structure (bold line with stars). Thin lines correspond to the results of Monte-Carlo calculations of the

absorption coefficient, which is shown on the left scale. The gain is negatives due to too high average doping concentration of the structures. Although the important point is that the absorption dependence on applied electric field agrees with the calculated one.

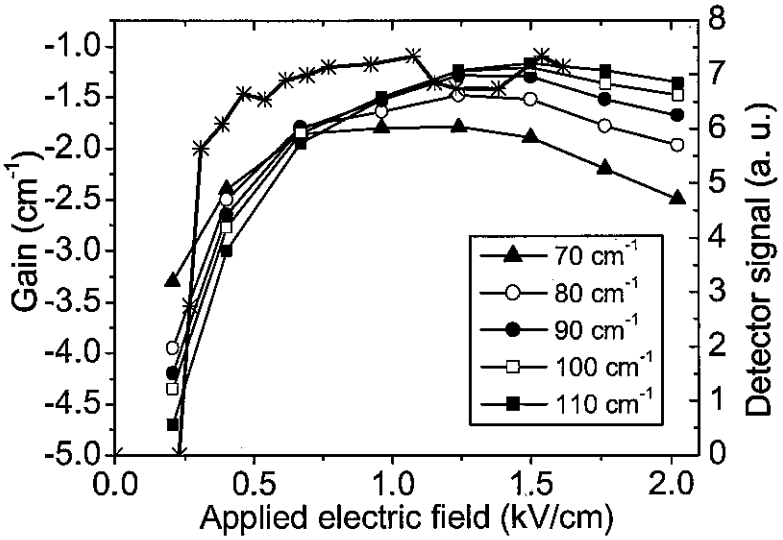


Fig.8 Measured intracavity laser transparency for the heavily doped structure. p-Ge laser signal as a function of the electric field applied to the structure (bold line with stars). The thin-lines are results of the calculations of the gain in the structures at different optical frequencies for the same configuration of applied fields as it is shown in Fig. 7. T=10 K, B=0.874 T, average hole concentration 4.3 x $10^{16}$ cm$^{-3}$, structure period 343 nm, width of the doped layers 31 nm.

## DISCUSSION AND CONCLUSION

We proposed theoretically and demonstrated with computer simulation an alternative way of creating an inversion population on direct optical transitions between light and heavy hole subbands in delta-doped structures, spatially separating light holes from ionized impurities and separating currents of light and heavy holes in the space. This eliminates light hole scattering on ionized impurities and on the majority of heavy holes, allowing an increase of light hole concentration to 1-3 x $10^{14}$ cm$^{-3}$, which is 10 times higher than the typical gain in bulk p-Ge lasers. Due to these high gain estimates, we anticipate the possibility of 77K operation.

The higher gain in the delta-doped Ge structures will permit smaller active volume than for bulk p-Ge lasers. The planar geometry facilitates heat extraction. Better cooling will allow higher duty and potential CW operation. The simplicity and low growth precision requirements allow chemical vapor deposition (CVD), which can produce structures of remarkable active thickness. We already demonstrated grown structures thicker than 30 μm. Due to homo-epitaxial nature of the structure and an absence of hetero-interfaces, growth of 100-150 μm thick structures without remarkable defect concentrations appears feasible. Such structures would be suitable for making low-loss confocal cavities for the spectral range 2-4 THz.

## APPENDIX:

Accurate treatment of carrier-carrier scattering is essential for our simulations because high average carrier concentration is a goal. Previous authors [1,6] have treated hole-hole scattering in p-Ge as an additional impurity scattering by taking the sum of acceptor and mobile carrier concentration as an effective impurity concentration. However, we find that carrier-carrier scattering has remarkably different angle-dependent scattering probabilities than impurity scattering. In particular, they are different for light-on-light and light-on-heavy hole scattering, which define light hole lifetime and achievable inversion population. Therefore, accurate treatment of carrier-carrier scattering, which

is necessary for optimization of our laser design, requires that it be treated separately and distinct from impurity scattering.

Coulomb interaction mediates scattering of holes on holes, and it is well known that scattering probability in a Coulomb potential diverges at small scattering angles (large impact parameter). Since small angle scattering does not cause inter-sub-band transitions (see below), it may be ignored or at least limited by some sort of screening. In this work we have chosen Yukawa or Debye-Huckel type screening with a characteristic screening length $\beta$. At low concentrations ($\leq 5 \times 10^{15}$ cm$^{-3}$) we used inverse Debye screening length. At higher concentration, third-body interference has to be introduced according to statistical screening method [7]. Since small-angle scattering does not contribute to intersubband transition rates (see below), results presented here will not depend on the screening model or the way of eliminating the divergence of the total scattering cross section. The carrier-carrier transition rate for $\vec{k}_1 + \vec{k}_2 \Rightarrow \vec{k}_3 + \vec{k}_4$ can be calculated as

$$P_{1,2\to 3,4} \cong \frac{2\pi}{\hbar}\left|\left\langle \Psi_{3,4}\left|\frac{e^2 \exp(-\beta r)}{4\pi\varepsilon\varepsilon_0 r}\right|\Psi_{1,2}\right\rangle\right|^2 \delta(E_1 + E_2 - E_3 - E_4), \tag{1}$$

where $\vec{k}_i$ – hole wavevector, $\hbar$ – Planck constant, e – electron charge, $\beta$ – screening parameter, $\varepsilon$ – relative dielectric constant, $\varepsilon_0$ – permittivity of free space, and $E_i$ – hole kinetic energy. The symmetrized two-particle wavefunctions are

$$\Psi_{i,j}(\vec{r}) = \frac{1}{\sqrt{2}}\left\{\psi_i(\vec{r}_i)\psi_j(\vec{r}_j) \pm \psi_i(\vec{r}_j)\psi_j(\vec{r}_i)\right\}, \tag{2}$$

where $\psi_i(\vec{r}_i)$ – single hole wavefunction in i-th state. Holes in a perfect crystal are described by Bloch wavefunctions

$$\psi_{v,\vec{k}}(\vec{r}) = \frac{1}{\sqrt{N}} u_{v,\vec{k}}(\vec{r}) \exp(i\vec{k}\cdot\vec{r}), \tag{3}$$

where v is the band index, $\hbar\vec{k}$ is the quasi momentum of the hole, $u_{v,\vec{k}_v}(\vec{r})$ is a function with the periodicity of the crystal, and N is the number of unit cells of volume $V_u$ in the crystal. Substituting (2) into (1) we obtain transition rates, which have inter and intra- sub-band overlap factors defined as

$$G_{i,j}(\vec{k}_i, \vec{k}_j) = \left|\int_V u^*_{j,\vec{k}_j}(\vec{r}) u_{i,\vec{k}_i}(\vec{r}) d\vec{r}\right|^2. \tag{4}$$

If valence band warping is neglected, which is a good approximation for germanium, these factors for intra- and inter-subband scattering can be calculated as [8]

$$G_{i,j}(\vec{k}_i, \vec{k}_j) \approx \left\{\begin{array}{ll} \frac{1}{4}(1+3\cos^2\theta) & i = j \\ \frac{3}{4}\sin^2\theta & i \neq j \end{array}\right\}, \tag{5}$$

where $\theta$ is the angle between $\vec{k}_i$ and $\vec{k}_j$.

According to (5), the scattering angle should be close to $\pi/2$ for intersubband scattering ($i \neq j$) to occur. Small angle scattering tends to maintain the hole in the same sub-band. Figs. 9 and 10 show angular dependence of the rate ($s^{-1}$) for single scattering events. In both cases, each incident hole has kinetic energy 20 meV, effective masses and dielectric parameters are those of germanium, and hole concentration is $10^{14}$ cm$^{-3}$. For such a low concentrations, rates are linearly proportional to the concentration. In Fig. 9, a light hole collides with a heavy hole and makes a transition to the heavy subband (L+H–>H+H). The directions of the incident hole wavevectors are indicated by solid arrows. For these fixed directions, the final wavevectors can have any directions consistent with conservation of momentum $\vec{k}_1 + \vec{k}_2 = \vec{k}_3 + \vec{k}_4$ and energy $E_1 + E_2 = E_3 + E_4$. One possible set of final wavevector directions is shown as dashed lines in Fig. 9. The different possible final directions have different probabilities, as indicated by the shading contours on the surface of the sphere. Fig. 10 shows the situation when a heavy hole collides with another heavy hole and makes a transition to the light subband (H+H–>L+H). In order to change its sub-band, the hole must be deflected significantly from its original direction. As one can see from the Figs. 9-10, intersubband hole-hole scattering has

stronger angular dependence compared to ionized impurity scattering. Because of much larger effective mass, the heavy hole usually tends to keep its momentum direction closer to total momentum direction of the system when colliding with light hole (see Fig. 9). The black bulls-eye around the original direction of the heavy hole in Fig. 10 is because of forbidden intersubband transition for small-angle scattering events. This forbidden region of directions appears also on the surface map for the second hole because of the momentum conservation.

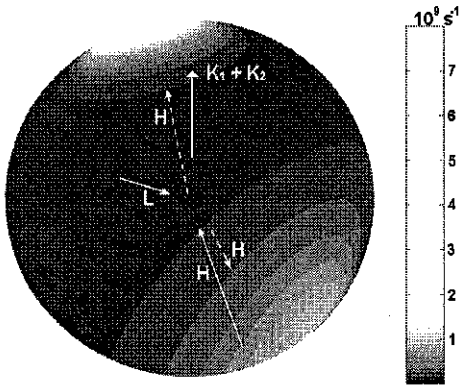


Fig. 9 Angular dependence of inter-band hole-hole scattering for light-to-heavy hole transition in L+H–>H+H process. Initial kinetic energies are $E_1 = E_2 = 20$ meV, hole concentration is $10^{14}$ cm$^{-3}$. The solid arrows are chosen fixed incident momentum directions. The dashed lines represent one possible scattering outcome. Probability of different outcomes is indicated by shading of the sphere.

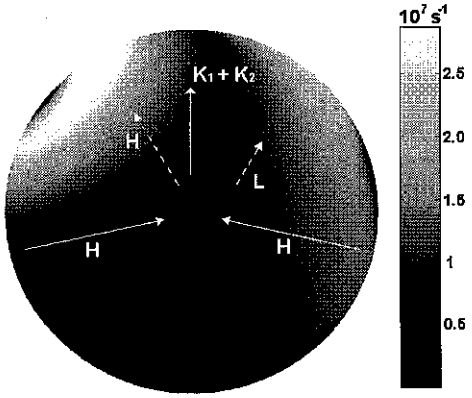


Fig. 10 Angular dependence of inter-band hole-hole scattering (s$^{-1}$) for heavy-to-light hole transition in H+H–>L+H process. Initial kinetic energies are $E_1 = E_2 = 20$ meV, hole concentration is $10^{14}$ cm$^{-3}$. The solid arrows are chosen fixed incident momentum directions. The dashed lines represent one possible scattering outcome. Probability of different outcomes is indicated by shading of the sphere.

Figs. 11 and 12 show scattering rates as a function of one of the incident hole directions (dashed arrow) for fixed direction of the other incident hole (solid arrow). The integration is over all possible final states of the scattered holes with indicated final subbands. In each figure both incident holes have kinetic energy 20 meV, and rate values correspond to a hole concentration of $10^{14}$ cm$^{-3}$. Fig. 11 is for the process L+H–>H+H where the incident light hole suffers a transition to the heavy hole subband. The shading of the sphere indicates that the total probability for a L+H–>H+H process has a maximum when the incident particles are moving in the same direction. This is when they interact for the longest time. Nevertheless, the rate for this process is very high for nearly all angles between incident particles.

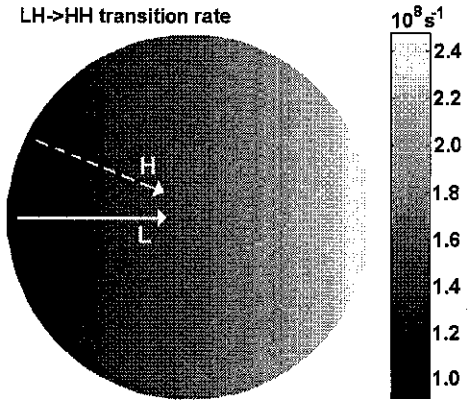


Fig. 11 Light-to-heavy inter-band transition rate as a function of the second (heavy) hole initial motion direction (dashed line). Initial kinetic energies are $E_1 = E_2 = 20$ meV, hole concentration is $10^{14}$ cm$^{-3}$. Rates have been integrated over final momentum.

Fig. 12 is for the process H+H–>L+H, where one of the incident heavy holes is promoted to the light hole subband. The shading on the sphere indicates that this process is more likely when the two incident particles move toward each other in opposite directions. Moreover, Fig. 12 shows that promotion of one heavy hole to the light hole band in a collision between two heavy holes is impossible unless the angle between incident momentum directions exceeds $\pi/2$ (note choice of hole directions in Fig. 10).

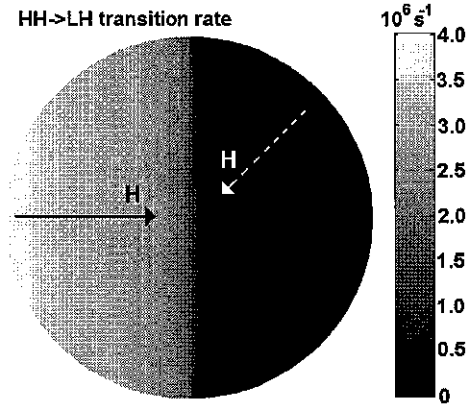


Fig. 12 H+H–>L+H inter-sub-band transition rate as a function of the second hole initial motion direction (dashed line). Initial kinetic energies are $E_1 = E_2 = 20$ meV, hole concentration is $10^{14}$ cm$^{-3}$. Rates have been integrated over final momentum.

The striking difference in angular dependence between the L+H–>H+H and H+H–>L+H processes revealed in Figs. 11 and 12 is a consequence of conservation laws and the large difference in effective mass between light and heavy holes. The maximum rate for the latter (inversion building) process is much less than that for the former (inversion destroying) process.

Total inter- and intra- subband scattering probabilities will also strongly depend on the kinetic energies of the interacting holes. In contrast, ionized impurity scattering depends on only one kinetic energy parameter. Because of the angular dependence, described in Figs. 9-12, hole-hole scattering rates depend on the angular part of the light and heavy hole distribution functions in momentum space. The less isotropic the carrier distribution function is, the more hole-hole scattering differs from ionized impurity scattering. For strongly anisotropic distribution functions, like in the hot-hole p-Ge laser, scattering rates and lifetimes associated with them can be significantly different compared to ionized impurity scattering, and the usual approach with doubled effective ionized impurity concentration that has been used for p-Ge

laser simulations (see [1,6]) is not correct for situations with high local concentrations, where ionized impurity and hole-hole are the main scattering mechanisms.

## ACKNOWLEDGMENTS

This work was partially supported by AFOSR contracts F49620-02-C-0025 and F49620-02-C-0027.

## REFERENCES

1. V. N. Shastin, "Hot hole inter-sub-band transition p-Ge FIR laser", Opt. Quantum Electron., 23, S111 (1991).
2. M.V. Dolguikh, A. V. Muravjov, and R. E. Peale, "Selectively doped germanium THz laser", Proc. SPIE 5411, 207, (2004).
3. M.V. Dolguikh, A. V. Muravjov, and R. E. Peale, "Intravalence-band THz laser in selectively-doped semiconductor structure", Proc. SPIE 5365, 184 (2004).
4. R. Kohler, A. Tredicucci, F. Beltram, H. E. Beere, E. H. Linfield, A. G. Davies, D. A. Ritchie, R. C. Iotti, and F. Rossi, "Terahertz semiconductor-heterostructure laser", Nature 417, 156 (2002).
5. M. Rochat, L. Ajili, H. Willenberg, J. Faist, H. Beere, G. Davies, E. Linfield, and D. Ritchie, "Low threshold terahertz quantum-cascade laser", Appl. Phys. Lett. 81, 1381 (2002).
6. E.V.Starikov, P.N.Shiktorov, "Numerical simulation of far infrared emission under population inversion of hot sub-bands", Optical and Quantum Electronics, 23, S177 (1991).
7. B. K. Ridley, "Reconciliation of the Conwell-Weisskopf and Brooks-Herring formulae for charged-impurity scattering in semiconductors: Third-body interference", J. Phys. C: Solid State Phys.,10, p. 1589, (1977).
8. J. D. Wiley, "Polar mobility of holes in III-V compounds", Phys. Rev. B 4, 2485 (1971).